Rare Metal Materials and Engineering
Volume 50, Issue 11, November 2021
Available online at www.rmme.ac.cn

Science Press

Cite this article as: Wu Zhuangzhi, Chen Hao, Cai Zhenyang, et al. Finite Element Simulation of Stress Distribution and Crack Propagation of $MoSi_2$/Mo Coating During Thermal Shock Cycles[J]. Rare Metal Materials and Engineering, 2021, 50(11): 3934-3941.

ARTICLE

Finite Element Simulation of Stress Distribution and Crack Propagation of $MoSi_2$/Mo Coating During Thermal Shock Cycles

Wu Zhuangzhi, Chen Hao, Cai Zhenyang, Liu Xinli, Wang Dezhi

School of Materials Science and Engineering, Central South University, Changsha 410083, China

Abstract: The thermal shock behavior of molybdenum disilicide ($MoSi_2$)/molybdenum (Mo) coating and the crack propagation were evaluated by heating the coating to 1000 °C, and then cooling it down to room temperature under the protection atmosphere of hydrogen during the thermal shock cycle. Meanwhile the thermal stress distribution of $MoSi_2$/Mo coating during thermal shock was calculated by Abaqus software. The development process of crack during thermal shock cycles was discussed. The results show that there is a high thermal shock stress between the Mo substrate and $MoSi_2$ coating, which can lead to the crack initiation and propagation. According to the extended finite element simulation results, the cracks appear perpendicular to the interface during the first ten thermal shock cycles, while the coating is still well bonded with the substrate and shows no signs of crack along the interface. The interfacial crack appears in the subsequent thermal shock cycles. The interfacial crack begins at the end zone of the vertical crack. When the vertical crack and the interfacial crack converge, the coating peels off and the coating failure occurs.

Key words: $MoSi_2$ coating; thermal shock; finite element simulation; stress distribution

Refractory molybdenum alloys are considered as one of the most promising structural material due to their superior properties at high temperature, such as high melting point of 2620 °C, good electrical conductivity, excellent thermal conductivity, great mechanical properties, and fine corrosion resistance[1,2]. Molybdenum and its alloys are widely applied in electronics, metallurgy, and nuclear industry fields. They have also been used as the emitter of space thermionic reactor, missile nozzle, satellite rocket booster, aero engine blade, and high-temperature electrode[3,4]. However, molybdenum has a poor oxidation resistance in air when the surrounding temperature is 600 °C. The molybdenum after oxidation can easily form several oxides, such as MoO_3 and MoO_2[5,6]. Therefore, the development of oxidation-resistant coatings is helpful to improve the oxidation resistance of molybdenum and its alloys[7-9].

Among many anti-oxidation coatings, $MoSi_2$ is the most suitable for the Mo alloys because it has favorable high temperature stability, such as the high melting point of 2030 °C and low density of 6.24 g/cm^3. In addition, it can form a protective self-healing glass to fill the cracks and pores on the surface, which further prevents the contact between oxygen and the substrate at high temperature[10-12]. However, the cracks are usually formed along the grain boundaries of the $MoSi_2$ coating during cooling stage[13]. The physical damage mechanism can be described as follows: the thermal shock generates the residual stress, which then induces the initiation and propagation of the cracks. The cracks occur with interfacial debonding or sliding. Many studies focused on the interfacial crack and vertical crack of the coating system. Hutchinson et al[14] described the mixed cracking mode in lamellar materials, and showed that the competition between interfacial crack propagation and interfacial kink depends on the relative toughness of the interface and the adjacent material. Zhou et al[15] investigated the effect of crack morphology on the interface fracture, and found that the shorter the crack length, the greater the crack density and the better the fracture resistance of the coating interface. Michlik et al[16] adopted the extended finite element method (XFEM) to

Received date: November 15, 2020
Foundation item: National Key R&D Program of China (2018YFC1901700)
Corresponding author: Liu Xinli, Ph. D., Associate Professor, School of Materials Science and Engineering, Central South University, Changsha 410083, P. R. China, E-mail: liuxinli@csu.edu.cn

simulate the crack appearance and calculate the equivalent Young's modulus of coating and the heat conductivity parameters of real cracks. Yan et al[17] studied the cracking and propagation mechanism of cracks among different layers in thermal barrier coating system. Mao et al[18] used the analytical method to study the change of residual stress in thermal barrier coating system under thermal shock cycles. Gilbert et al[19] conducted a numerical study on the damage of the coating under thermal shock in coating system. In fact, when the $MoSi_2$/Mo coating is served at high temperature, the difference in the elastic modulus and the thermal expansion coefficient between the layers may result in stress due to thermal mismatch, which is obvious during the heating and cooling stages. Although a great deal of research has been made on the interfacial crack and surface crack in the thermal barrier coating system, there are little research on the analysis of stress and crack of $MoSi_2$/Mo coating under thermal shock cycles. In this research, the thermal stress distribution was analyzed. XFEM and cohesive zone model (CZM) were used to simulate the $MoSi_2$ coating and the crack propagation during thermal shock, respectively. CZM is one of the most common methods for interface failure simulation[20]. Through XFEM, the crack propagation path does not need to preset. The crack can propagate freely under the stress instead of propagating along the mesh boundaries by forcing, and in fact the cracks can penetrate the mesh during the propagation process. Moreover, the sparse mesh can obtain high-precision numerical results. These advantages of XFEM are the reasons why this method is so active in the field of computing science over the past decade[21]. Therefore, the thermal stress distribution and crack initiation and propagation during thermal shock cycles were analyzed by XFEM, and the results were also confirmed by the experiment.

1 Experiment

The $MoSi_2$ coating was prepared by slurry sintering method[22]. Pure molybdenum plate was used as the substrate for coating experiments. Before coating, the plate was polished, ultrasonically cleaned, dried, and finally sandblasted. Then, the binder powder of Mo, Si, and polyvinyl butyral (PVB) with the mass ratio of 30: 69.5: 0.5 was prepared. The ethanol was used as the solvent and mixed with the binder powder by high-energy ball milling. Then the obtained slurry was sprayed uniformly onto the Mo plate. After sintering in a high-purity Ar atmosphere at 1450 °C for 60 min, the Si-Mo coating was prepared. Scanning electron microscopy (SEM, FEL Quanta 250 FEG) was used to observe the cross-sectional microstructure of the specimens and the crack initiation and propagation process. Fig. 1 presents the SEM image and the X-ray diffraction (XRD) patterns of the Mo substrate and the coating. The coating consists of $MoSi_2$ phase (Fig.1b), and its thickness is about 40 μm. The thermal shock cycles of the $MoSi_2$/Si coating were conducted in a tube furnace heated by electrical resistance and protected by hydrogen to prevent oxidation. The specimens were heated to 1000 °C in 10 min, and then cooled down to the room temperature. The above process was regarded as one cycle. The coating specimens were taken out from the tube furnace after thermal shock of 10 and 30 cycles.

The simulation procedure was consistent with the practical procedure. The commercially available Abaqus software was used to simulate the thermal shock cycles. The model based on the structure of $MoSi_2$/Mo coating was established, and the thickness of the substrate and coating were set as 5 and 0.04 mm, respectively. The XFEM was applied to simulate the arbitrary crack propagation in $MoSi_2$ coating[23], and the CZM was applied to investigate the degradation of interface debonding[24]. In order to save the computation time, a simplified asymmetrical model was adopted, as shown in Fig. 2[25]. The CZM was inserted between the substrate and coating, and the initial cracks in the coating were prefabricated on the coating surface.

Displacement boundary conditions were used to restrict the displacement along *X* and *Y* directions on the left and bottom of the coating system, respectively. The mesh in the important part was fine enough. The denser the mesh, the more accurate the simulation result. However, when the mesh was too dense, the computation time would be extremely long. Temperature was selected as the driving force of the crack propagation, and the initial temperature was set as 20 °C. The elements of coating and substrate are CPE4R with the mesh size of 0.008 and 0.1 mm, respectively, and the interface was meshed by a single layer of cohesive elements of COH2D4. There were 13 753 elements in total after meshing.

The thermal physical parameters of Mo substrate and $MoSi_2$ coating involved in the simulation are shown in Table 1~6[26-28]. In this research, all the work was based on the

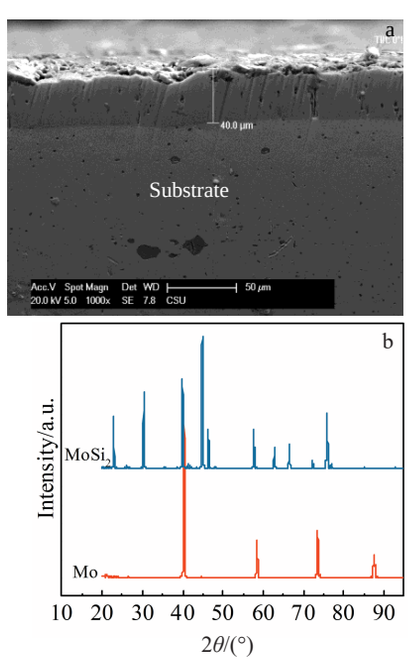

Fig.1 SEM image (a) and XRD patterns (b) of Mo substrate and $MoSi_2$ coating

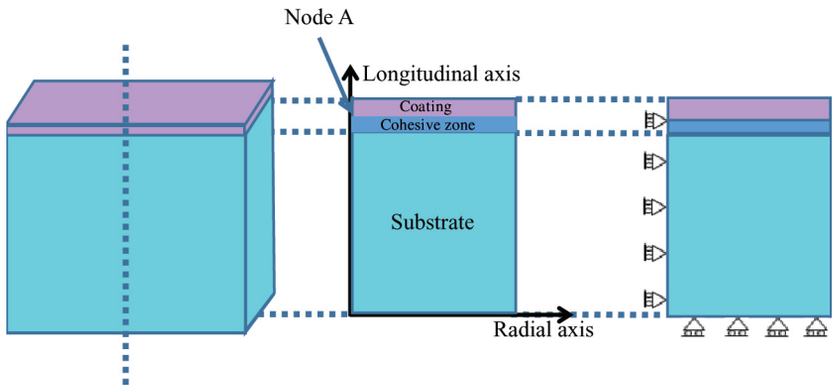

Fig.2 Simplified asymmetrical model used in XFEM simulation[25]

following assumptions: (1) the properties of the $MoSi_2$/Mo coating were considered to be linear elastic; (2) the effect of the oxidation and creep behavior was not considered in the simulation process.

2 Results and Discussion

2.1 Stress development and distribution in $MoSi_2$/Mo coating during thermal shock cycles

Fig. 3 presents the stress distribution of $MoSi_2$/Mo coating after 10 and 30 thermal shock cycles. It shows that after 10 thermal shock cycles, the maximum radial tensile stress is located at the left of the top coating, because the left edge is constrained and lacks displacement degrees of freedom.

Table 1 Coefficient of thermal conductivity of Mo substrate and $MoSi_2$ coating ($W \cdot K \cdot m^{-1}$)

Temperature/°C	Mo	$MoSi_2$
20	142.00	25
25	135.29	-
200	116.27	-
400	114.95	-
600	110.43	-
800	106.69	-
1000	105.00	-

Table 2 Young's modulus of Mo substrate and $MoSi_2$ coating (GPa)

Temperature/°C	Mo	$MoSi_2$
20	311.16	425
100	307.84	-
200	303.64	-
300	299.46	-
400	295.28	-
500	291.10	-
600	286.92	-
700	282.74	-
1000	270.00	-

Table 3 Thermal expansion coefficient of Mo substrate and $MoSi_2$ coating ($\times 10^{-6}$ °C^{-1})

Temperature/°C	Mo	$MoSi_2$
20	4.90	8.1
100	5.13	-
200	4.97	-
300	5.49	-
400	5.60	-
500	5.70	-
600	5.95	-
700	6.28	-

Table 4 Plasticity of Mo substrate (MPa)

Temperature/°C	Mo
25	560
300	365
800	290
1200	105

Table 5 Specific heat of Mo substrate and $MoSi_2$ coating ($J \cdot kg^{-1} \cdot K^{-1}$)

Temperature/°C	Mo	$MoSi_2$
20	250.20	420.74
25	287.66	-

Table 6 Poisson's ratio of Mo substrate and $MoSi_2$ coating

Temperature/°C	Mo	$MoSi_2$
20	0.38	0.15

Meanwhile the top coating suffers the severe tensile stress and leads to the development of micro-cracks which are propagated vertically towards the surface coating, especially on the left edge of the surface coating. It can be also seen that the maximum radial stress in different thermal shock cycles is basically the same. After 10 and 30 thermal shock cycles, the maximum radial stress is 445 MPa.

The maximum axial tensile stress can be located at the right

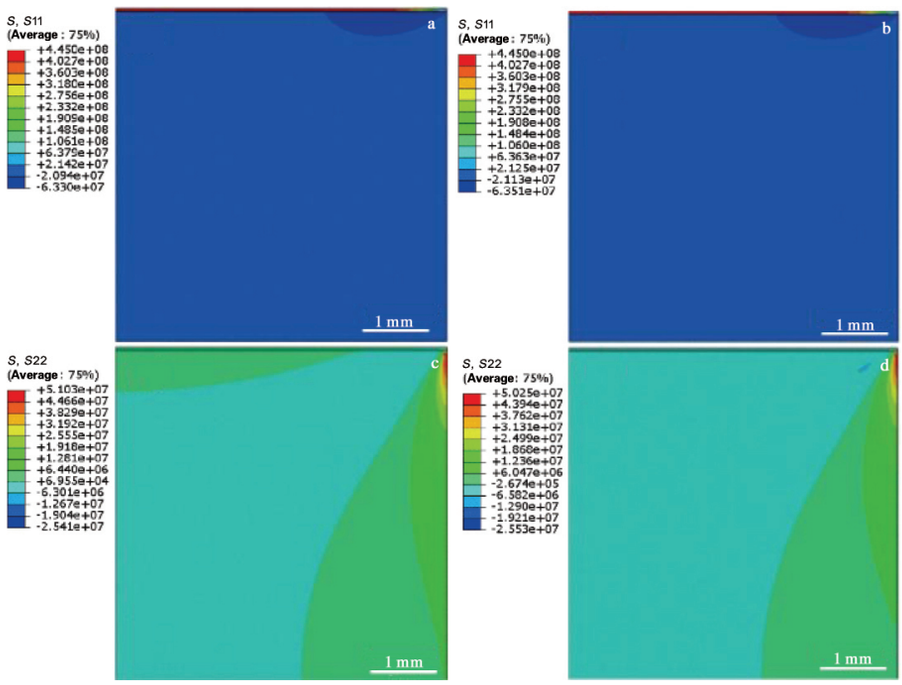

Fig.3 Radial stress (a, b) and axial stress (c, d) distributions of $MoSi_2$/Mo coating after 10 (a, c) and 30 (b, d) thermal shock cycles

edge below the interface. Compared with the radial stress, there is no stress gradient in the coating and the magnitude is much lower. With increasing the thermal shock cycles, the maximum stress does not change much. Since the axial displacement boundary condition is applied, only the radial stress needs to be discussed. Fig.4a shows the radial stress of node A (Fig. 1) with increasing the number of thermal shock cycles. It can be seen that the maximum radial tensile stress of node A reaches 442 MPa, and the maximum radial compressive stress reaches 290 MPa. The maximum tensile stress and compressive stress nearly remain the same value from the second thermal shock cycle to the 30th thermal shock cycle. As shown in Fig. 4b, during the initial heating stage, the max principle stress is 0; while during the cooling stage, the max principle stress rapidly increases to 630 MPa and keeps the similar variation trend in each subsequent cycle. The max principle stress concentration is generated at the left part of the top coating, and the max principle stress is considered as the damage criterion of the coating crack. So, the coating crack appears at the left part of the top coating which suffers from the maximum radial stress at the same time. A vertical crack can be expected in the left part of the coating. In conclusion, the radial stress in the top coating is much more severe than that of the substrate.

Failure of the $MoSi_2$/Mo coating is associated with the accumulated stress, which is mainly due to the thermal expansion mismatch and temperature gradient. When the specimen is taken out from the high temperature zone and enters a cooling zone during the thermal shock process, a very large stress occurs at the interface due to the difference in thermal expansion coefficients between the substrate and the coating, which can be expressed as follows:

$$\sigma_f = \frac{E_f \Delta\alpha \Delta T}{1 - \nu_f^2} \quad (1)$$

where σ_f is stress in the coating; E_f and ν_f are Young's modulus

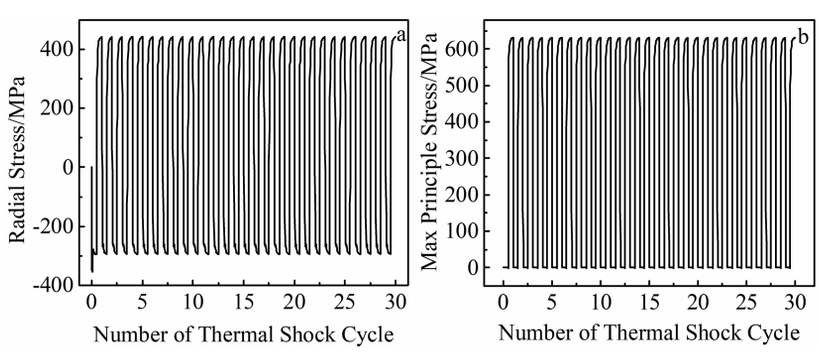

Fig.4 Radial stress (a) and max principle stress (b) of node A

and Poisson ' s ratio, respectively; $\Delta\alpha$ is the difference in thermal expansion coefficients between the coating and the substrate; ΔT is the change in temperature. The linear expansion coefficients of Mo substrate and $MoSi_2$ coating are 4.9×10^{-6} and 8.1×10^{-6} K^{-1}, respectively. Due to the difference in thermal expansion coefficient, the thermal stress occurs during thermal shock cycles. Meanwhile, the increase in temperature gradient may result in the thermal stress. In addition, the high strain energy is gradually accumulated in the coating due to thermal stress. When the strain energy exceeds the limit of strain capacity of the coating, cracks originating from the defects can propagate along the grain boundaries, which leads to the formation of vertical cracks in the coating.

Fig. 5 presents the axial tensile stress distribution along the radial axis. It can be seen that the coating is subjected to very high stress, indicating that the crack can easily develop at this position.

2.2 Influence of crack on thermal shock behavior of coating system

The cracks produced during the coating preparation process have a strong impact on the whole coating system, which also influences the thermal shock behavior. The occurrence of the cracks inside the coating is mainly due to the brittleness of ceramic coating. Based on the above discussion, cracks are inevitable during the preparation process.

Fig. 6 displays the crack propagation process under stress. As shown in Fig. 6a, there is a small existing crack on the coating surface. It can be seen from Fig. 6b that the crack begins to grow in the first cooling stage, and the stress in the crack tip reaches 508.5 MPa. When the coating specimen is heated to a high temperature, the stress decreases; when the coating specimen is cooled to a low temperature, the stress increases. Fig. 6d and 6e show that the stress increases from 471.3 MPa to 501.6 MPa at the crack tip in the second cooling stage. The crack continues to grow in the subsequent thermal cycles, and it eventually penetrates the coating, forming a vertical crack, as shown in Fig.6f.

The damage and failure of the interface cohesive element is determined by the stiffness degradation rate (SDEG). The value range of SDEG is 0~1. When SDEG is 0, it indicates that the cohesive element is intact without any damage. When SDEG reaches 1, the corresponding cohesive element fails off and cracks appear in the damage area. After the first heating stage, the crack in the coating cannot be propagated. But during the cooling stage, the crack tip generates stress concentration. When the stress reaches the stress failure criterion, the crack begins to grow along the direction of the maximum stress[29], so the vertical crack appears. In the next cooling stage, the vertical crack has an influence on the interfacial crack. Previous studies[30,31] also showed that the vertical cracks can exert a strong impact on the interfacial crack. When the coating has a certain crack density, the prefabricated vertical crack has a certain dissipation effect on the thermal load of the interface. Furthermore, the crack can absorb the energy for creating the interfacial crack, which suppresses the generation of cracks at the interface and results in less damage to the interface.

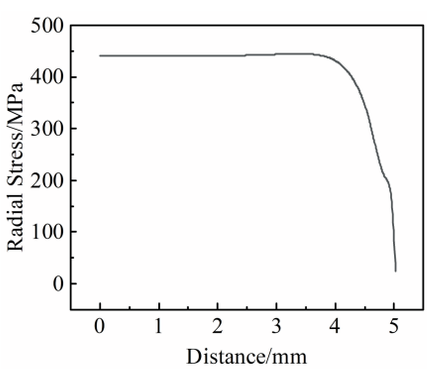

Fig.5 Radial stress distribution along radial axis at cohesive zone of coating surface after 30 thermal shock cycles

However, when the crack grows to a certain length, the vertical cracks encourage the degradation of the interface. Fig. 7b shows that the interface stiffness is 0.333 and the interface begins to be damaged. When the coating system cools down from 1000 °C to room temperature, the vertical cracks penetrate the coating. $MoSi_2$ is a brittle ceramic material without yield phenomenon. When the stress on the coating reaches the max principal stress criterion, the cracks are generated in the coating. According to Fig. 4b, the max principal stress does not change with increasing the number of thermal shock cycles. The max principal stress reaches 630 MPa in the first thermal cycle. The damage to the coating is generated in the first thermal shock cycle, and then the interfacial crack begins to grow on both ends due to the influence of the vertical crack. In the subsequent heating stage, the maximum SDEG reaches 0.916, as shown in Fig.7c. The damage degree of the coating becomes larger, and the damage range becomes wider in the subsequent thermal shock cycles. After 10 thermal shock cycles, the coating maintains the vertical crack, the interface remains intact, and no crack appears. With further increasing the number of thermal shock cycles, the interfacial crack is generated and propagated toward both ends. The interfacial cracks have great influence on the coating performance, including the decrease of coating adhesion and the confluence of several vertical cracks and interfacial cracks, which results in coating failure and the exposure of substrate in the working environment. Fig. 7e shows the cross-sectional morphology of the coating after 10 thermal shock cycles. It can be seen that there is an obvious vertical crack and the interface bonding, which is consistent with the simulation results in Fig. 7c. Fig. 7f shows the cross-sectional morphology of the coating after 30 thermal shock cycles. The vertical crack and interfacial crack converge, leading to the peeling of coating, which is consistent with the simulated result in Fig.7d.

2.3 Influence of thermal shock on multiple crack propagation

In order to investigate the influence of thermal shock on

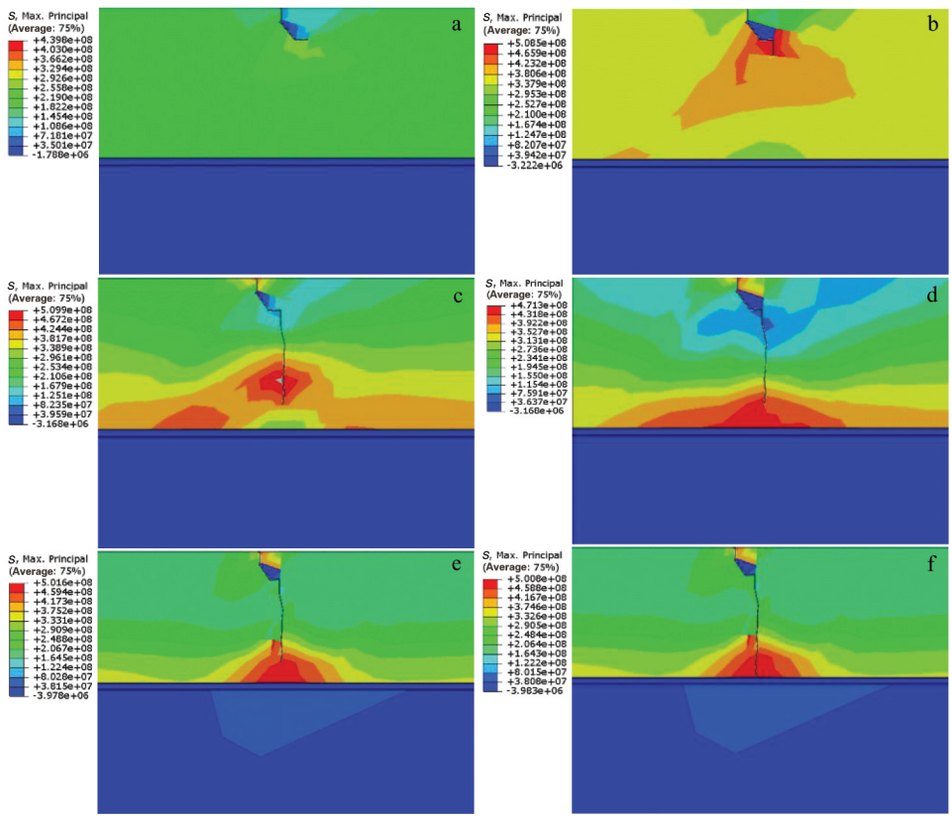

Fig.6 Max principle stress distributions of crack tip during crack propagation: (a) crack occurrence in the first cooling stage; (b) crack growth in the first cooling stage; (c) cessation of crack growth after the first cooling stage; (d) crack occurrence in the second cooling stage; (e) crack growth in the second cooling stage; (f) crack penetrating into substrate

multiple crack propagation, three cracks were prefabricated on the coating surface and the distances between the cracks were 0.5 and 2 mm. The three cracks are named as A, B, and C from left side to right side. As shown in Fig.8, when the crack spacing is 0.5 mm, the time required for crack A to penetrate the coating is 2079 s, but the other two cracks are not propagated. When the crack spacing is 2 mm, the crack B is propagated and the propagation time is 3201.9 s. Meanwhile, compared with that of specimen with the crack spacing of 0.5 mm, the propagation time of crack A is greatly reduced to 736 s. In these two cases, the crack C is not propagated. In general, with the same number of cracks, the larger the spacing, the less the propagation time for cracks to penetrate the coating. This is because the energy for crack propagation is the same. The larger the crack spacing, the smaller the mutual influence between each crack[32]. The time required for crack propagation depends not only on the thermal shock condition, but also on the spacing between cracks.

3 Failure Mechanism of $MoSi_2$/Mo Coating

The failure of coatings is influenced by many factors, such as the roughness and the bonding strength of the interface. When the coating is subjected to external thermal load, the stress can be concentrated in the trough and peak firstly, which are the positions where cracks are generated as well. Then, with the thermal shock process continuing, the cracks in the trough and peak converge, causing damage to the coating[33]. Some studies showed that when the coating is subjected to the mechanical load, with increasing the interface roughness, the tensile stress and maximum tensile stress near the peak and trough of the interface can be increased at the same time. The smoother the interface, the better the suppression effect against the crack[34].

When the bonding strength of the interface is lower than that of the substrate, before the crack reaches the interface, the interface begins to fail[35].

In this research, only the influence of thermal stress caused by temperature change on the coating failure is considered. Because of the difference in thermal expansion coefficients between substrate and coating, the thermal stress accumulates, and the high thermal stress finally leads to the coating failure. According to the experiment and simulation results, the vertical crack firstly appears in the coating, because the radial stress is greater than the axial stress. But vertical cracks in the coating induce the interfacial cracks. When the multiple cracks appear in the coating, the order of crack propagation is from left side to right side because the stress is mainly distributed on the left side of the model. It can be seen from the simulation results that the cracks in the coating can influence each other.

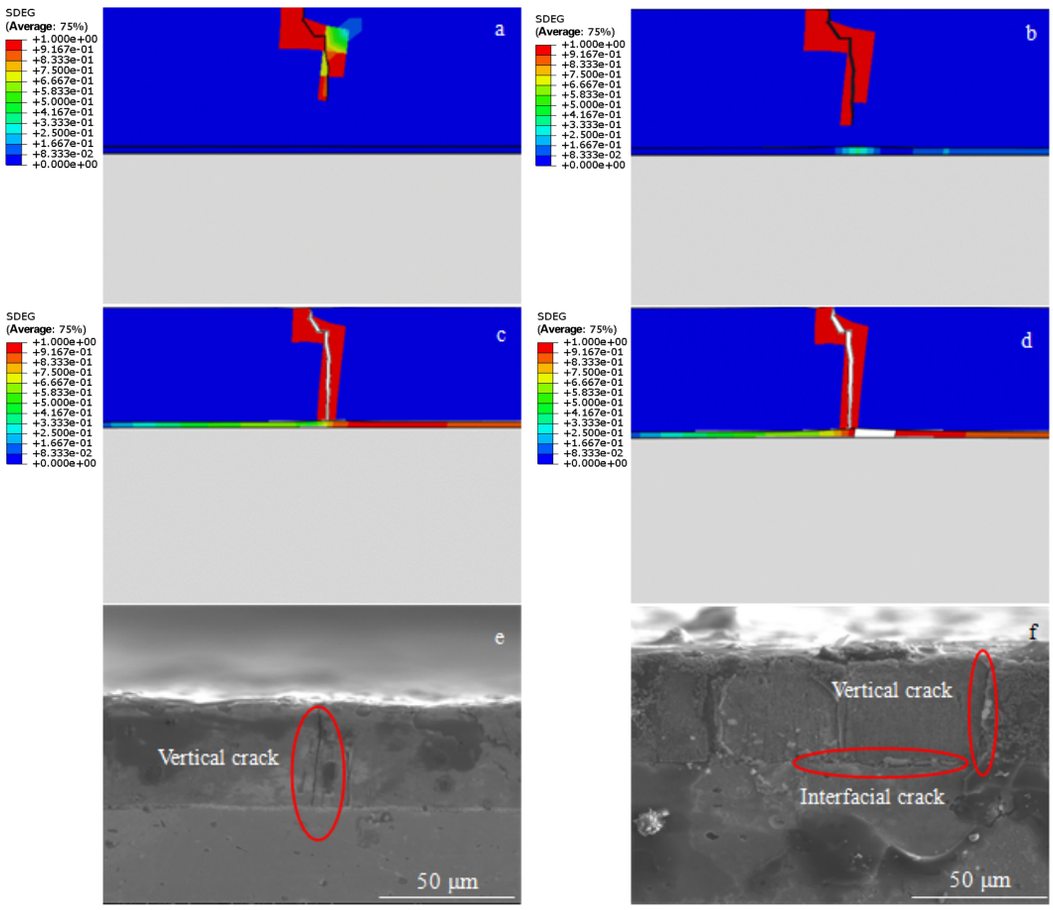

Fig.7 Simulated morphologies of crack propagation process during thermal shock cycles: (a) the beginning stage, (b) the growing stage, (c) after 10 thermal shock cycles, and (d) after 30 thermal shock cycles; actual morphologies after 10 thermal shock cycles (e) and after 30 thermal shock cycles (f)

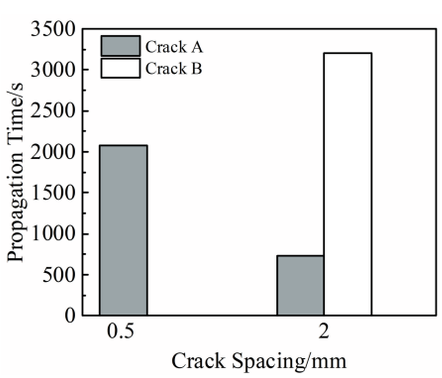

Fig.8 Propagation time of cracks penetrating the coating with different crack spacings

4 Conclusions

1) The maximum radial tensile stress is located at the left part of the top coating. The radial stress in the top coating is much more severe than that of the substrate.

2) During the thermal shock cycles, the vertical crack firstly appears in the coating, and it can be propagated with increasing the number of the thermal shock cycles. The vertical crack can also suppress the initiation of the interfacial crack. But when the crack grows to a certain length, it encourages the initiation of the interfacial crack.

3) With the same number of cracks, the larger the crack spacing, the less the propagation time for cracks to penetrate the coating.

References

1 Monteverde F. *Materials Chemistry and Physics*[J], 2009, 113(2-3): 626

2 Tang Sufang, Deng Jingyi, Wang Shijun *et al*. *Materials Science and Engineering A*[J], 2007, 465(1): 1

3 Zee R H, Xiao Z, Chin B A *et al*. *Journal of Materials Processing Technology*[J], 2001, 113(1): 75

4 Vasuévan A K, Petrovic J J. *Materials Science and Engineering A* [J], 1992, 155(1-2): 1

5 Fei X A, Niu Y R, Jia H *et al*. *Ceramics International*[J], 2010, 36(7): 2235

6 Ingemarsson L, Hellström K, Canovic S *et al*. *Journal of*

Materials Science[J], 2013, 48(4): 1511
7 Zhang Yingyi, Li Yungang, Bai Chengguang. *Ceramics International*[J], 2017, 43(8): 6250
8 Deng Xinke, Zhang Guojun, Wang Tao *et al*. *Ceramics International*[J], 2019, 45(1): 415
9 Cai Zhengyang, Wu Yonghuang, Liu Huyun *et al*. *Materials and Design*[J], 2018, 155: 463
10 Yoon J K, Kim G H, Byun J Y *et al*. *Surface and Coatings Technology*[J], 2003, 165(1): 81
11 Zhang H A, Gu S Y. *International Journal of Refractory Metals and Hard Materials*[J], 2013, 41(11): 128
12 Liu Z D, Hou S X, Liu D Y *et al*. *Surface and Coatings Technology*[J], 2008, 202(13): 2917
13 Yoon J K, Kim G H, Han J H *et al*. *Surface and Coatings Technology*[J], 2005, 200(7): 2537
14 Hutchinson J W, Suo Z. *Advances in Applied Mechanics*[J], 1992, 29(8): 63
15 Zhou B, Kokini K. *Materials Science and Engineering A*[J], 2003, 348(1-2): 271
16 Michlik P, Berndt C. *Surface and Coatings Technology*[J], 2006, 201(6): 2369
17 Yan J, Leist T, Bartsch M *et al*. *Acta Materialia*[J], 2008, 56(15): 4080
18 Mao W G, Zhou Y C, Yang L *et al*. *Mechanics of Materials*[J], 2006, 38(12): 1118
19 Gilbert A, Kokini K, Sankarasubramanian S. *Surface and Coatings Technology*[J], 2008, 203(1-2): 91
20 Dugdale D S. *Journal of the Mechanics and Physics of Solids*[J], 1960, 8(2): 100
21 Belytschko T, Black T. *International Journal for Numerical Methods in Engineering*[J], 1999, 45(5): 601
22 Cai Z Y, Liu S N, Xiao L R *et al*. *Surface and Coatings Technology*[J], 2017, 324: 182
23 Fu Bin, Yang Xiaoxiang. *Journal of Fuzhou University*[J], 2018, 46(3): 386 (in Chinese)
24 Kyaw S T, Jones I A, Hyde T H. *The Journal of Strain Analysis for Engineering Design*[J], 2016, 51(2): 132
25 Chen Hao, Wu Zhuangzhi, Liu Xinli *et al*. *China Molybdenum Industry*[J], 2021, 45(2): 55 (in Chinese)
26 Fang Shuangquan, Huang Qunhua, Qiao Yingjie *et al*. *Heat Treatment of Metals*[J], 2009, 34(8): 7 (in Chinese)
27 Zhou Xiya, Fang Peiyu. *China Ceramics*[J], 2006, 42(2): 19 (in Chinese)
28 Pan You. *Thesis of Master*[D]. Harbin: Harbin Institute of Technology, 2019 (in Chinese)
29 Schulze G W, Erdogan F. *International Journal of Solids and Structures*[J], 1998, 35(28-29): 3615
30 Jiang Wugui, Zou Hang, Xia Mufeng *et al*. *Surface Technology* [J], 2019, 48(1): 30 (in Chinese)
31 Lu Z, Kim M S, Myoung S W *et al*. *Transactions of Nonferrous Metals Society of China*[J], 2014, 24(S1): 29
32 Yu Qingmin, Shi Yongzhi. *Rare Metal Materials and Engineering*[J], 2018, 47(10): 3052 (in Chinese)
33 Wang Libin, Yu Qingmin. *Rare Metal Materials and Engineering* [J], 2014, 43(12): 3095 (in Chinese)
34 Zhong Jianlan, Ao Bo, Gu Yuqi. *Rare Metal Materials and Engineering*[J], 2018, 47(7): 2100 (in Chinese)
35 Fu Yonghui. *Thesis of Master*[D]. Xi'an: Xi'an Jiaotong University, 2000

$MoSi_2$/Mo涂层热震过程中界面应力分布和裂纹扩展的有限元模拟

吴壮志，陈　浩，蔡圳阳，刘新利，王德志
(中南大学 材料科学与工程学院，湖南 长沙 410083)

摘　要：在氢气保护下将$MoSi_2$/Mo涂层加热至1000 ℃，再迅速冷却至室温进行热震循环，表征了材料在热震循环过程中裂纹的演变过程并评估了$MoSi_2$/Mo涂层的热冲击行为。采用Abaqus软件计算了$MoSi_2$/Mo涂层在热冲击过程中的应力分布，讨论了热震循环中裂纹的发展过程。结果表明：Mo基体与$MoSi_2$涂层之间存在较高的热冲击应力，这将导致裂纹的萌生和扩展。计算结果显示：在最初的10次热震循环中，涂层产生了垂直于界面的裂纹，在界面上没有出现裂纹，涂层与基体仍结合良好；在随后的热震循环中开始出现界面裂纹，界面裂纹开始于垂直裂纹的末端区域，当垂直裂纹与界面裂纹汇聚，会导致涂层剥离和涂层失效。

关键词：$MoSi_2$涂层；热冲击；有限元模拟；应力分布

作者简介：吴壮志，男，1984年生，博士，教授，中南大学材料科学与工程学院，湖南 长沙 410083，E-mail：zwu2012@csu.edu.cn